Primljen / Received: 10.3.2024.
Ispravljen / Corrected: 27.2.2025.
Prihvaćen / Accepted: 5.3.2025.
Dostupno online / Available online: 10.7.2025.

Seismic behavior of telescopic buckling braced frame structure

Authors:

Xiaowei Yang, PhD. CE
Zhongyuan University of Technology, China
School of Intelligent Construction and Civil Engineering
yxw43@163.com
Corresponding author

Yiqiong Zhang, MSc. CE
Zhongyuan University of Technology, China
School of Intelligent Construction and Civil Engineering
z0611yq@163.com

Mengyuan Li, MSc. CE
Zhongyuan University of Technology, China
School of Intelligent Construction and Civil Engineering
lmy3977@163.com

Research Paper

Xiaowei Yang, Yiqiong Zhang, Mengyuan Li

Seismic behavior of telescopic buckling braced frame structure

A telescopic buckling brace was investigated. The design method for the brace was established, and finite element simulations were conducted. The simulation accuracy was validated against the existing test results, and an elastoplastic dynamic time history analysis method was used to study the seismic performance of the telescopic buckling brace frame structure. The results showed that under the action of strong earthquakes, compared with ordinary braced frame structures, the shape of the base shear-vertex displacement hysteresis curve of the telescopic buckling frame structure was relatively full, the seismic energy dissipation capacity was increased by 34 %, and the base shear force of the structure was reduced by 23 %. The maximum floor displacement and the maximum story drift angle of the structure were reduced by 20 %.

Key words:
frame structure, telescopic buckling braced, elastoplastic dynamic time history analysis, seismic performance

Prethodno priopćenje

Xiaowei Yang, Yiqiong Zhang, Mengyuan Li

Seizmičko ponašanje teleskopski dijagonalno pridržanog okvira

Istraženo je ponašanje teleskopskoga dijagonalnog elementa za pridržanje protiv izvijanja. Utvrđena je metoda projektiranja takvog elementa te su provedene numeričke simulacije metodom konačnih elemenata. Točnost simulacija potvrđena je usporedbom s postojećim eksperimentalnim rezultatima. Za analizu seizmičkog ponašanja konstrukcije okvira s teleskopskim dijagonalnim elementima za pridržanje protiv izvijanje primijenjena je metoda nelinearne dinamičke analize odziva. Rezultati su pokazali da pod djelovanjem jakih potresa, a u usporedbi s konvencionalnim okvirima s dijagonalnim ukrućenjem, okvir s teleskopskim dijagonalnim elementima ima znatno puniji oblik petlje histereze koja pokazuje odnos ukupne posmične sile u razini temelja i pomaka vrha konstrukcije, pri čemu je kapacitet disipacije seizmičke energije povećan za 34 %, a ukupna posmična sila u razini temelja smanjena za 23 %. Maksimalni međukatni pomaci i maksimalni međukatni kutovi zaokreta smanjeni su za 20 %.

Ključne riječi:
okvirna konstrukcija, teleskopski dijagonalni element za pridržanje protiv izvijanja, nelinearna dinamička analiza odziva, seizmičko ponašanje

1. Introduction

Structures under strong earthquakes dissipate earthquake energy through deformation and damping. Owing to the small inherent damping of structures, strong earthquakes cause most structural members to exhibit stiffness and strength degradation. Therefore, installing damping devices in certain controlled parts of a building structure is an effective and economical approach to improve the seismic performance of a structure. This allows the plastic deformation of the damping devices to dissipate most of the seismic energy and prevent structural component damage. Tamahloult et al. [1] conducted a study on the analysis and design of the nonlinear seismic response of multistory buildings isolated with lead-rubber bearings under near-field earthquake conditions. The results indicated that the isolation system exhibited an excellent seismic performance while satisfying the shear strain and stability requirements. Kandemir et al. [2] employed the wavelet coherence technology to determine the optimal size of viscous dampers and conducted an in-depth analysis to determine the effectiveness of application of nonlinear viscous dampers in mitigating earthquake effects. Zhou et al. [3] investigated the behaviour of embedded perforated steel plate composite shear walls under seismic loading, revealing significant energy dissipation capabilities of the structural system. Buckling-restrained bracing is a suitable choice for improving the stiffness of structures and dissipating energy via damping. Clark et al. [4] conducted three large-scale buckling-restrained bracing experiments that provided a technical brace for the structural design and construction of the first building with buckling-restrained bracing in the United States. Luo et al. [5] and Cheng at al. [6] demonstrated through experiments and simulations that a buckling-restrained energy-dissipating brace can provide sufficient lateral stiffness and stable energy dissipation capacity for a structure. The greater the ratio of the yield load of the buckling-restrained energy-dissipating brace to the weight of the structure, the longer the structural period, and the more significant the effect of the buckling-restrained energy-dissipating brace. Li et al. [7] utilised domestic Q235B steel to fabricate buckling-restrained energy-dissipating braces and experimentally validated their stiffness and energy dissipation capabilities. Despite their effectiveness, the manufacturing processes of these brace components are relatively complex. Baird et al. [8] investigated the passive energy-dissipation effects of U-shaped steel plates used as connected buckling dampers. Building on this foundation, Chen et al. [9] developed a telescopic buckling brace using U-shaped steel plates. However, these dampers exhibited the drawback of asymmetric reciprocating bearing forces after yielding. Consequently, as substitutes for U-shaped curved plates, this study proposes the use of elliptical steel pipes arranged in series and parallel to develop a telescopic buckling brace. The effectiveness of the developed brace is evaluated in passive seismic energy dissipation within a structure.

2. Telescopic buckling brace design

2.1. Telescopic buckling brace

The core structure of a telescopic buckling brace is shown in Figure 1. The connecting endplates with mounting holes on both sides were connected to the structural members, producing a relative displacement to form a lateral force-damping energy-dissipation system. When the telescopic buckling brace member was under tension or compression, the connecting end plates at both ends caused the outer-frame steel plate and core plate to slide relative to each other into the gap because of the elliptical steel pipes connecting them. Displacement was generated, and the bending yield of the arc section of the elliptical steel pipe was effectively utilised, providing effective damping and energy dissipation.

2.2. Theoretical analysis of telescopic buckling brace

Kelly et al. [10] derived the following equations for the yield bending moment and bearing capacity of an arc section of a semicircular steel plate, as shown in Figure 2.a:

$$M_p = \frac{f_y b_u t_u^2}{4} \tag{1}$$

$$F_p = \frac{2M_p}{D_u} = \frac{f_y b_u t_u^2}{2D_u} \tag{2}$$

where M_p is the yield bending moment at the arc section, F_p is the yield force at the arc section, f_y is the yield strength of the steel, D_u is the diameter between the thickness centres of the arc section, b_u is the Width of the U-shaped steel plate section, t_u is the thickness of the arc section, and r_u is the radius of the arc section centre.

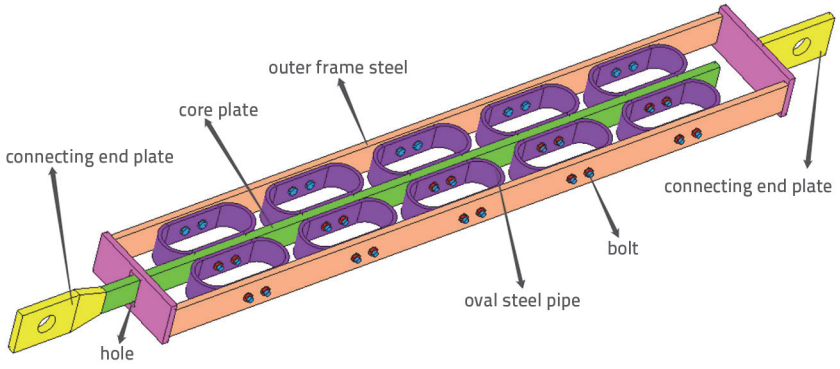

Figure 1. Structure of the telescopic buckling brace

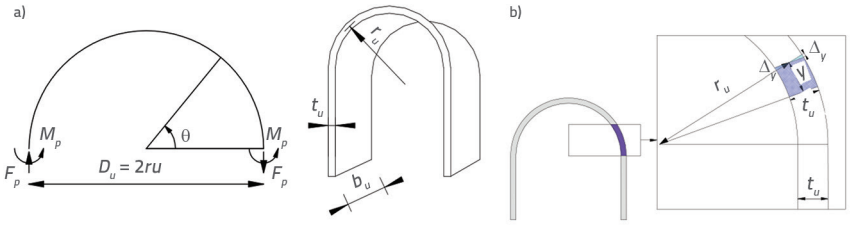

Figure 2. Mechanical analysis of arc section: a) Schematic diagram of forces on arc section; b) schematic diagram of arc section deformation

Under the action of force F_p, the semi-circular steel plate underwent a bending deformation that was consistent with that of a flat section. That is, when the outer edge of the arc section undergoes compression or elongation deformation (Δ_y), the inner edge of the arc section must also produce elongation or compression deformation (Δ_y), as shown in Figure 2.b. Thus, the geometric relationship shows that the maximum strain is equal to thickness divided by diameter.

$$\varepsilon_{\max} = \frac{t_u}{D_u} \tag{3}$$

The yield displacement (Δ_y) of the arc-shaped section of the semicircular steel plate can be calculated by the energy method according to Castigliano's second theorem, Liu [11]:

$$\Delta = \frac{\partial U}{\partial F} \tag{4}$$

The strain energy U in Eq. (4) is mainly produced by bending and can be calculated using the integral of the squared bending moment, Liu [11]:

$$U = \int_0^L \frac{M_p^2(x)}{2EI} \tag{5}$$

where E is the modulus of elasticity of the steel and I is the moment of inertia of the section of the steel plate, defined as $I = b_u t_u^3 / 12$.

As shown in Figure 1.a, the bending moment ($M(\theta)$) of the arc section at angle θ between the semicircular steel plate and the end is obtained as follows:

$$M(\theta) = F_P r_u (1 - \cos\theta) + F_P r_u \tag{6}$$

Eqs. (5) and (6) were substituted into Eq. (4) to obtain the following expression for the yield displacement Δ_y:

$$\begin{aligned}\Delta_y &= \int_0^L \frac{\partial}{\partial F} \frac{[F_P r_u (1-\cos\theta) + F_P r_u]^2}{2EI} r_u \partial\theta \\ &= \frac{27\pi F_P D_u^3}{16 E b_u t_u^3} = \frac{27\pi f_y D_u^2}{32 E t_u}\end{aligned} \tag{7}$$

Therefore, the initial stiffness (k_0) can be defined as follows:

$$k_0 = \frac{F_P}{\Delta_y} = \frac{16 E b_u}{27\pi}\left(\frac{t_u}{D_u}\right)^3 \tag{8}$$

The yield bearing capacity (F_b), yield displacement (Δ_y), and initial stiffness k_b of the telescopic buckling brace shown in Figure 1 are calculated as follows:

$$F_b = 2nF_P = \frac{n f_y b_u t_u^2}{D_u} \tag{9}$$

$$\Delta_y = \frac{27\pi f_y D_u^2}{32 E t_u} \tag{10}$$

$$\begin{aligned}k_b &= \frac{32 n E b_u}{27\pi}\left(\frac{t_u}{D_u}\right)^3 \\ &\approx \frac{1.2 n E b_u}{\pi}\left(\frac{t_u}{D_u}\right)^3\end{aligned} \tag{11}$$

where n is the number of oval steel pipes.

To ensure the effective application of the damper and to prevent damage to the steel plate from excessive deformation and overloading, the following limits were established for the ultimate bearing capacity (F_u, hardening coefficient was 1.4) and ultimate displacement (Δ_u) of the steel during design calculations:

$$F_u = 1{,}4\, F_b \tag{12}$$

$$\Delta_u = 3\Delta_y \tag{13}$$

The force-displacement skeleton curve is based on the Ramberg-Osgood model (Chegini, [12]):

$$\Delta = \frac{F}{k_0}\left[1 + \left(\frac{F}{F_y}\right)^{R-1}\right] \tag{14}$$

$$R = 7.1 \ln\left(\frac{t_u}{D_u}\right) + 29.5 \tag{15}$$

where R is a dimensionless parameter that determines the shape of the curve.

2.3. Experiment and numerical analysis

To verify the hysteretic energy dissipation performance of the telescopic buckling brace shown in Figure 1, experiments were conducted using a U-shaped steel plate test model (Chegini [12]) and finite element simulations of half of the symmetric elliptical steel pipe. In the finite element model shown in Figure 3, the radius (r_u) of the U-shaped steel plate was 65 mm, thickness (t_u) was 6 mm, width (b_u) was 150 mm, length (l_u) was 220 mm, and the diameter of the two bolt holes was 16 mm. The steel was modelled using an elastoplastic double-broken-line strengthening model (Figure 3.c). The steel grade

was G300, elastic modulus E was 205 GPa, Poisson's ratio ν was 0.3, yield strength f_y was 320 MPa, and hardening coefficient was 1.4.

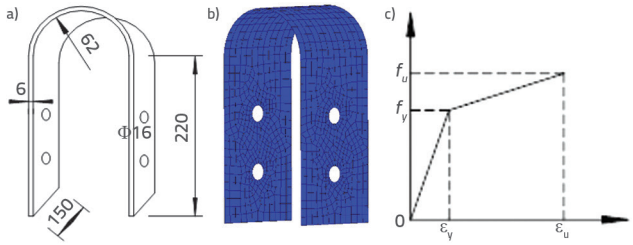

Figure 3. U-shaped steel plate and finite element method (FEM) model: a) U-shaped steel plate (Chegini [12]); b) FEM model; c) Stress-Strain Relationship of Steel

The calculation results are shown in Figure 4. The skeleton line results from the experiments, finite element simulations, and theory are essentially the same. The theoretical calculation of the skeleton curve can be utilised to determine the component design parameters by omitting 2n from equations (9) and (11). Additionally, finite element analysis can serve as a substitute for experimental testing in simulations. Therefore, the finite element model of the telescopic buckling brace shown in Figure 1 was established for the low-cycle reciprocating numerical experiments, as shown in Figure 5.

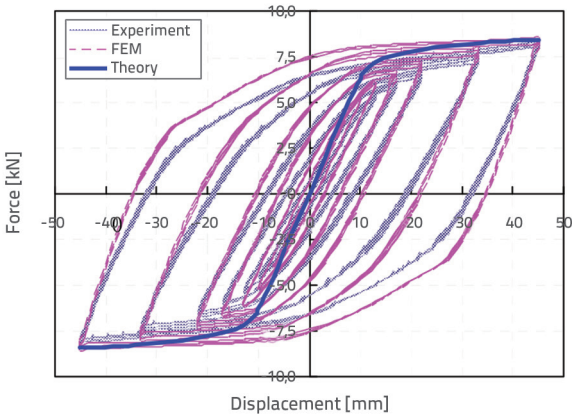

Figure 4. Comparison of hysteresis curves. FEM, finite element method

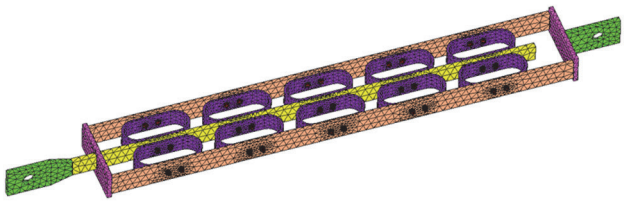

Figure 5. Finite element method (FEM) model of scalable buckling-restrained brace

An elliptical steel pipe was fabricated by connecting two semi-circular steel plates with diameters (D_u) of 120 mm, thicknesses (t_u) of 22 mm, and widths (b_u) of 50 mm through a steel plate with a length (l_u) of 180 mm. Steel grade was Q345, the elastic modulus (E) of the steel was 206 GPa, the Poisson's ratio (ν) was 0.3, and the yield strength (f_y) was 345 MPa. An elastic-plastic double-line strengthening model (Figure 3(c)) was adopted, and the strengthening coefficient was 1.4. The calculation results are presented in Figure 6. The outcomes of the finite element analysis are largely consistent with the theoretical skeleton curve derived from equations (9) to (13). In the SAP2000 program (SAP2000 Technical Guide and Engineering Application, 2018), the theoretical parameters were employed to configure the Wen plastic link element to simulate the damper, as shown in Figure 1. The ratio of the post-yield stiffness to the elastic stiffness was set to 0.1, and the exponent index was assigned a value of 6. The simulation results are presented in Figure 6. The hysteresis curve simulated by the link element is similar to the finite element calculation results. In the structural model, a link element can be used instead of a damper for the calculations and simulations.

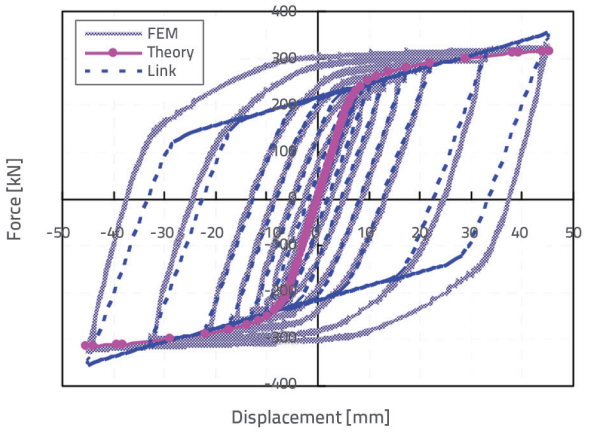

Figure 6. Force-displacement hysteresis curve of damping device. FEM, finite element method

3. Seismic performance of telescopic buckling brace frame structure

3.1. Design of telescopic buckling brace

A five-story reinforced concrete frame brace structure was designed according to the Chinese building structure design codes [14, 15].The plan layout included six vertical spans with a column spacing of 9 m and three horizontal spans with column spacing of 6.9 m, 3, and 6.9 m. The height of the ground floor was 4.5 m, while those of the other floors were 3 m. The floor and roof constant loads were both 5.5 kN/m^2, and the floor and roof live loads were 3.5 kN/m^2 and 2.0 kN/m^2, respectively. The concrete strength grade was C30 and the steel reinforcement grade was HRB400. The seismic fortification intensity of the structure was eight degrees (0.2

g), the site category was Class II, and the design earthquake group was Group 1.

Folić et al. (2023) introduced a novel approach for assessing the earthquake response of five-story reinforced concrete (RC) frame system buildings, leveraging European codes by examining various damage index models. To investigate the seismic performance of telescopic buckling braces within frame structures, this study replaces the braces in the aforementioned RC frame structure (model-1) with telescopic buckling braces, thereby establishing model-2 (as illustrated in Figure 7). An elastoplastic dynamic time-history analysis was employed to evaluate the seismic responses of both model-1 and model-2 under the influence of the three seismic waves. In these models, the frame beams and columns are represented by fibre beam elements, braces by rod elements, floors by layered shell elements, and dampers are modelled using connecting elements. The first two natural frequencies of the models presented in Table 1 revealed similar fundamental periods, suggesting that the lateral stiffnesses of the two models were essentially equivalent.

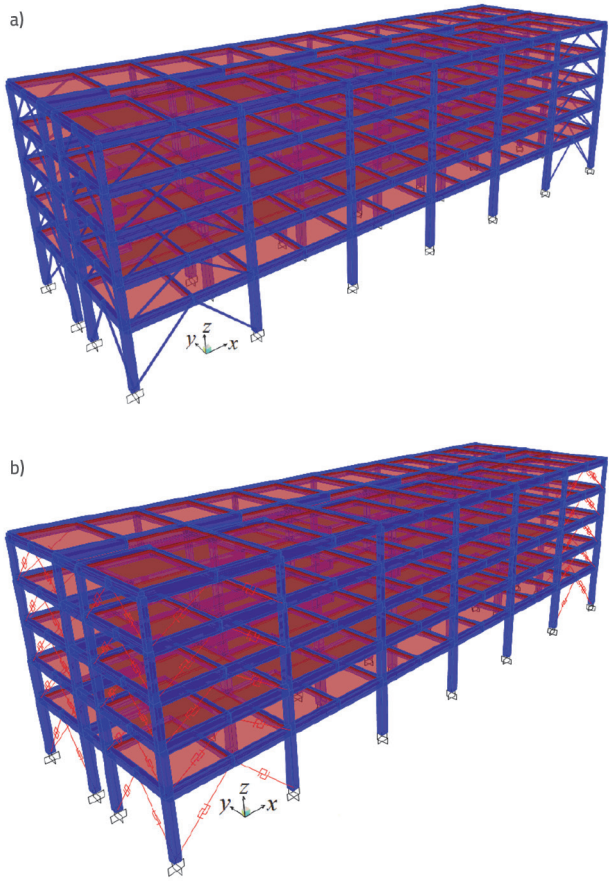

Figure 7. Elastic-plastic analysis models: a) Model 1; b) Model 2

Table 1. Basic periods of model-1 and model-2

Model		Model 1.	Model 2.	Razlika [%]
Temeljni period (s)	T_1	0,79	0,76	3,8
	T_2	0,74	0,72	2,7

3.2. Selection of seismic waves

According to the Code for the Seismic Design of Buildings [15], the three seismic waves shown in Figure 8 were selected. The comparison between the seismic wave response spectrum and the design response spectrum in the code at a 5 % damping ratio between 0.73 s and 0.8 s is shown in Figure 9. The three selected seismic waves satisfied the relevant code regulations.

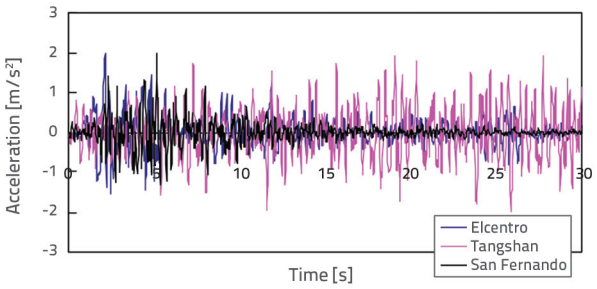

Figure 8. Time-history curves of three seismic waves

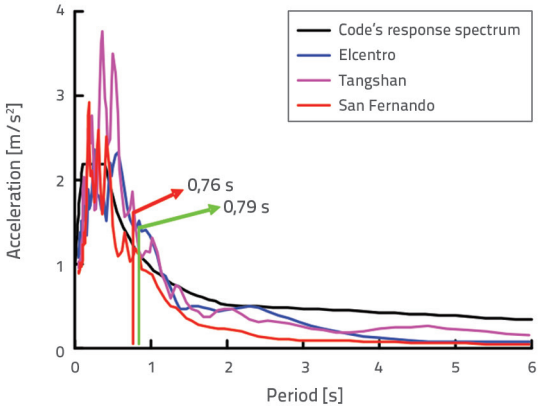

Figure 9. Response spectrum, a (m/s²), seismic influence coefficient

3.3. Seismic performance of telescopic buckling brace frame structure

3.3.1. Floor displacement and inter-story displacement angle

The maximum floor displacements of the structure under the action of the three seismic waves are shown in Figure 10. As shown in Figure 10.a, under a design earthquake and a maximum considered earthquake (the design values of seismic acceleration with two probabilities of exceedance in the 50-year design reference period: 10 % for a design earthquake and 2 % for

a maximum considered earthquake), the vertex displacements in the X-direction of model-1 were 73.2 mm and 146.3 mm, respectively, and the corresponding values of model-2 were 56.1 mm and 115.8 mm. The values of model-2 were 23.4 % and 20.8 % lower than those of model-1, respectively. As shown in Figure 10.b, under design earthquake and maximum considered earthquakes, the vertex displacements in the Y-direction of model-1 were 74.1 mm and 148.2 mm, respectively, and the corresponding values of model-2 were 59.8 mm and 120.6 mm. The values for model-2 were 19.3 % and 18.6 % lower than those for model-1, respectively.

The maximum story drift angles of the structures under the action of the three seismic waves are shown in Figure 11. As shown in Figure 11.a, under the fortified and maximum considered earthquakes, the maximum story drift angles in the X-direction of model-1 were 0.0058 (1 /172) and 0.012 (1/83), and the corresponding values for model-2 were 0.0045 (1/222) and 0.0092 (1/109), respectively. The values for model-2 were reduced by 22.4 % and 23.3 %, respectively, compared with those for model-1, respectively. As shown in Figure 11.b, under the fortified and maximum considered earthquakes, the maximum story drift angles in the Y-direction for model-1 were 0.0054 (1/185) and 0.011 (1/91), and the corresponding values for model-2 were 0.0047 (1/213) and 0.0095 (1/105), respectively. The values for model-2 were reduced by 13 % and 13.6 %, respectively, compared to those for model-1, respectively. The numerical results indicated that the telescopic buckling brace effectively reduced the maximum floor displacement and story drift angle of the structure under the action of fortified and maximum considered earthquakes.

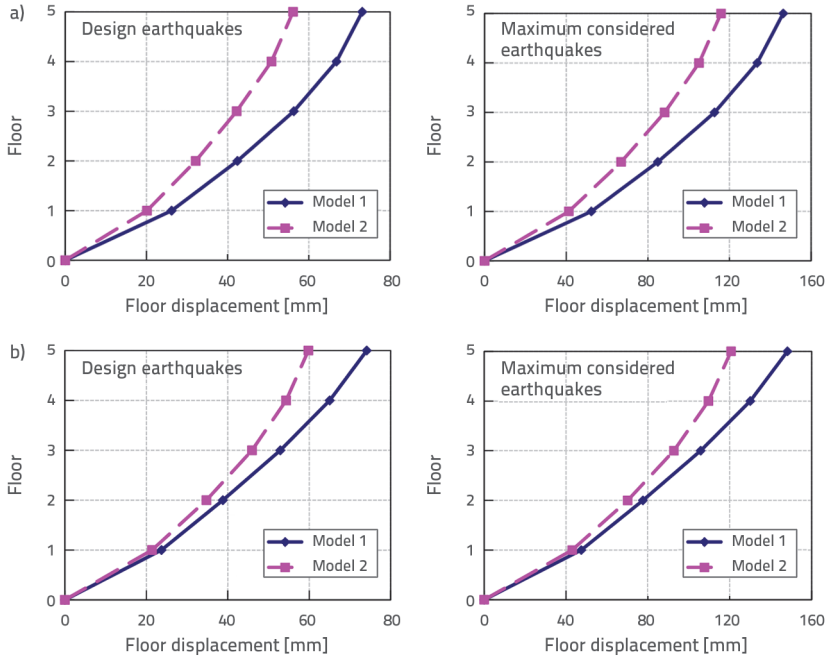

Figure 10. Maximum floor displacement under three seismic waves: a) X-direction; b) Y-direction

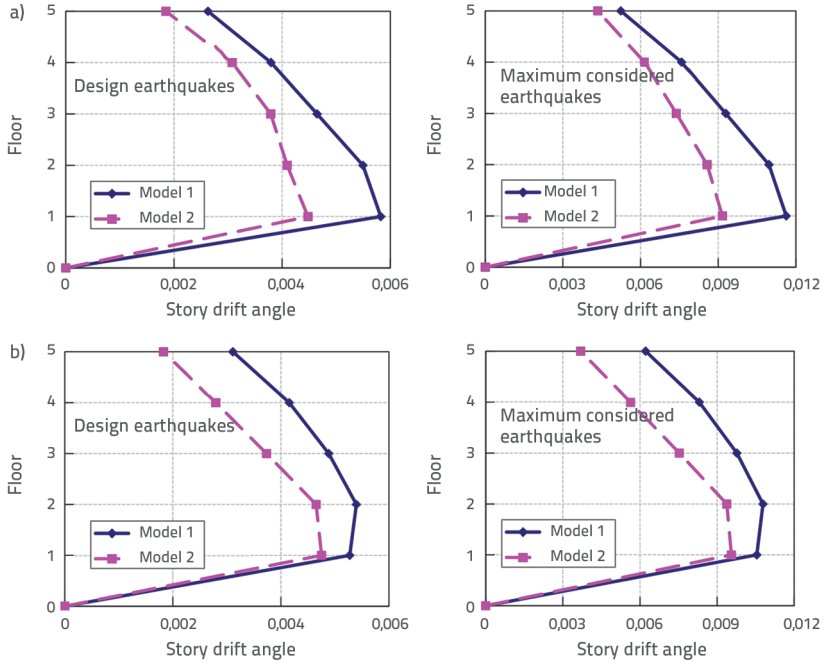

Figure 11. Maximum story drift angle under three seismic waves: a) X-direction; b) Y-direction

3.3.2. Base shear-vertex displacement curve

As shown in Figures 12 and 13, under the action of strong earthquakes, the base shear-vertex displacement hysteresis curve for model-2 was fuller than that for model-1, and the dissipation of seismic energy was better. Under the fortified and maximum considered earthquakes, the maximum base shear forces for model-1 in the X-direction were 22262 and 44525 kN, respectively, and the corresponding values for model-2 were 13611 and 26091 kN, respectively. The values for model-2 were 38.8 % and 41.4 % lower than those for model-1, respectively. Under the fortified and maximum considered earthquakes, the maximum

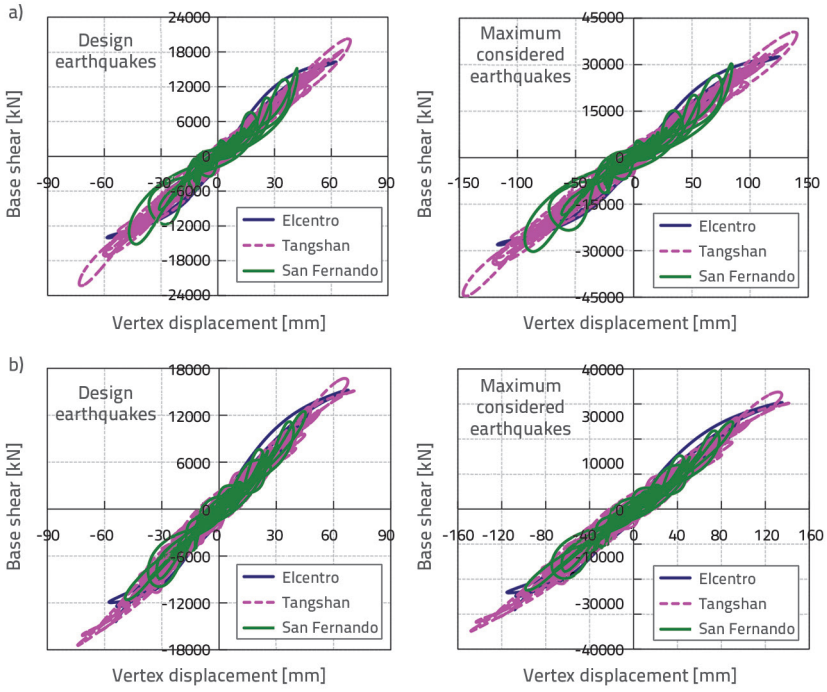

Figure 12. Base shear-vertex displacement curve of model-1: a) X-direction; b) Y-direction

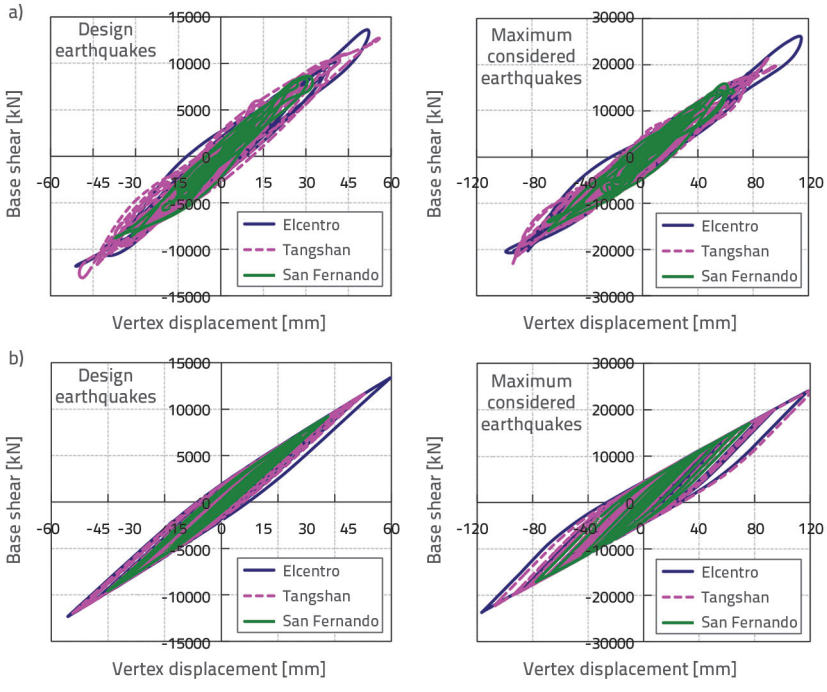

Figure 13. Base shear-vertex displacement curve of model-2: a) X-direction; b) Y-direction

shear force of the structure under the action of fortified and maximum considered earthquakes.

3.3.3. Damping energy dissipation of structural system

The force-displacement hysteretic curve of the damper within the structure subjected to earthquake waves is shown in Figure 14. Under the influence of both design-level and rare earthquakes, the hysteretic curve appears to be robust, indicating a significant capacity for dissipating seismic energy.

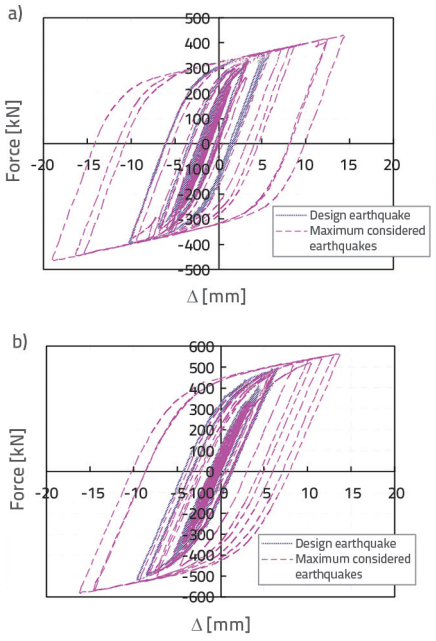

Figure 14. Force-displacement hysteretic curve of damper: a) X direction; b) Y direction

The average ratio of the damping energy consumption to the input energy of the structure under the action of the three seismic waves is shown in Figure 15. Under the action of the fortified and maximum considered earthquakes, the damping energy consumption in the X-direction of model-1 accounted for 64.9 % and 67.9 % of the total input energy, respectively, and the corresponding values for model-2 accounted for 88.5 % and 96.5 % of the total input energy, respectively. The energy consumption values for model-2 were 36.4 % and 42.1 % higher than those for model-1, respectively. Under the action of the fortified and maximum considered earthquakes, the damping energy consumption for model-1

base shear forces in the Y-direction for model-1 were 17445 and 34889 kN, respectively, and the corresponding values for model-2 were 13379 and 24773 kN, respectively. The values for model-2 were 23.3 % and 29 % lower than those for model-1, respectively. The numerical results indicate that the telescopic buckling brace can effectively reduce the seismic

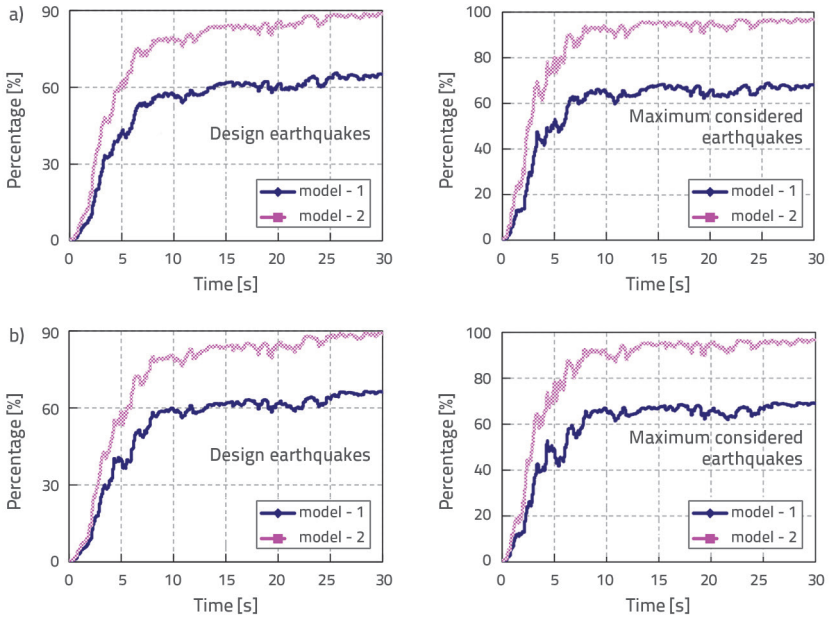

Figure 15. Average values of the ratio of the damping energy consumption to the input energy: a) X-direction; b) Y-direction

in the Y-direction accounted for 65.9 % and 68.8 % of the total input energy, respectively, and the corresponding values for model-2 accounted for 88.7 % and 96.4 % of the total input energy, respectively. The values of energy consumption for model-2 were 34.6 % and 40.1 % higher than those for model-1, respectively. The numerical results indicated that the telescopic buckling brace could play a beneficial role in damping and energy dissipation.

4. Conclusion

In this study, a telescopic buckling brace was investigated and its design methodology was proposed. The accuracy of the design was validated through a finite element analysis combined with existing experimental data. The seismic performance of telescopic buckling-braced-frame structures was examined using an elastoplastic dynamic time-history analysis method. The main conclusions are as follows:

- Theoretical analysis and numerical simulations indicated that the telescopic buckling brace could effectively utilise the bending yield of the curved section of an elliptical steel pipe when subjected to tension or compression, thereby demonstrating excellent damping and energy dissipation performance. The hysteretic curve of the brace is robust and its capacity to dissipate earthquake energy is significant. Under strong earthquakes, the foundation shear force and apex displacement of a structure can be effectively reduced.
- Under the design and maximum considered earthquake conditions, compared with the traditional reinforced concrete frame structure (model-1), the apex displacements and maximum interstory displacements in the X and Y directions of the structure were significantly reduced using telescopic buckling braces (model-2). This indicates that the brace effectively enhanced the lateral stiffness and seismic performance of the structure.
- Under strong earthquake conditions, the telescopic buckling brace significantly reduced the base shear force of the structure. The numerical simulation results show that the base shear force for model-2 was reduced by 38.8 % and 23.3 % in the X- and Y-directions, respectively, compared with that for model-1. This indicates that the brace can effectively share and dissipate earthquake energy during seismic events, thereby reducing the damage to structural components.
- In the event of the design and maximum considered earthquakes, the proportion of damping energy dissipation by the telescopic buckling braces relative to the total input energy was significantly higher than that by traditional structures. The numerical results demonstrate that the damping energy dissipation capacity of model-2 was 36.4 % and 34.6 % higher than that of model-1 in the X- and Y-directions, respectively. This indicates that the brace plays a significant role in energy dissipation during earthquakes, thereby further enhancing the seismic performance of the structure.

Acknowledgements

This study was financially supported by the Open Research Fund Project of the Institute of Structural Engineering, Shenzhen University (SZURISE: 2019-05). We gratefully acknowledge a scholarship under the State Scholarship Fund from the Structural Engineering Research Institute of Shenzhen University.

REFERENCES

[1] Tamahloult, M., Tiliouine, B.: 3D nonlinear seismic analysis and design of base-isolated buildings under near field ground motions, GRAĐEVINAR, 75 (2023) 5, pp. 483-493, https://doi.org/10.14256/JCE.3548.2022

[2] Kandemir, E.C.: Alternate approach for calculating the optimum viscous damper size, GRAĐEVINAR, 75 (2023) 2, pp. 153-162, https://doi.org/10.14256/JCE.3539.2022

[3] Zhou, Z., Cao, W., Liu, Y., Li, J.: Seismic behaviour of composite shear wall with steel reinforced concrete frame and embedded perforated-steel plate, GRAĐEVINAR, 74 (2022) 5, pp. 383-392, https://doi.org/10.14256/JCE.2770.2019

[4] Clark, P., Aiken, I., Kasai, K., Ko, E., Kimura, I.: Design procedures for buildings incorporating hysteretic damping devices, in: Proceedings of 68th Annual Convention, Santa Barbara, CA, USA, 1999, pp. 355-71.

[5] Luo, K., Cheng, S., Bai, X., Rong, W.: Analysis of mechanical behavior of the buckling restrained energy-dissipation braces (in Chinese), Earthq Resist Eng Retrofit, 29 (2007), pp. 23-27. https://doi.org/10.3969/j.issn.1002-8412.2007.02.005

[6] Cheng, G., Ye, L., Cui, H.: Study on the design method of buckling-restrained brace (in Chinese), J Build Struct, 29 (2008), pp. 40-48, https://doi.org/10.3321/j.issn:1000-6869.2008.01.006

[7] Li, G., Sun, F., Deng, Z., Guo, X., Jin, H.: Experimental study on the aseismic performance of buckling-restrained braces (in Chinese), Build Struct, 44 (2014), pp. 71-78.

[8] Baird, A., Smith, T., Palermo, A., Pampanin, S.: Experimental and numerical Study of U-shape Flexural Plate (UFP) dissipators, in: Proceedings of 2014 New Zealand Society for Earthquake Engineering Conference (NZSEE), Auckland, New Zealand, 2014, pp. P2.1-9.

[9] Chen, Y., Palermo, A., Mashal, M.: Cyclic tests of an innovative seismic bracing member-multiple U-shaped flexural plates dissipater in: Proceedings of 2020 New Zealand Society for Earthquake Engineering Conference (NZSEE), Auckland, New Zealand, 2020, pp. P2.1-189.

[10] Kelly, J.M., Skinner, R.I., Heine, A.J.: Mechanisms of energy absorption in special devices for use in earthquake resistant structures, Bull N Z Soc Earthq Eng, 5 (1972), pp. 63-88. https://doi.org/10.5459/bnzsee.5.3.63-88

[11] Liu, H.W.: Mechanics of Materials (in Chinese), 5th ed., Higher Education Press, Beijing, 2011.

[12] Chegini, Z.: Low-damage seismic design of bridge superstructures for accelerated bridge construction, University of Canterbury, Christchurch, New Zealand, 2018.

[13] Beijing Construction Information Solution Engineering Consulting, SAP2000 Technical Guide and Engineering Application, Chinese Version (in Chinese), China Communications Press, Beijing, 2018.

[14] GB 50011-2010: Code for seismic design of buildings (in Chinese). Ministry of Housing and Urban-Rural Construction, General Administration of Quality Supervision Inspection and Quarantine (2010).

[15] GB 50010-2010: Code for design of concrete structures (in Chinese). Ministry of Housing and Urban-Rural Construction, General Administration of Quality Supervision Inspection and Quarantine (2010).

[16] Folić, R., Čokić, M., Folić, B., Brujić, Z.: Damage assessment, fragility, and vulnerability analysis of reinforced concrete building, GRAĐEVINAR, 75 (2023) 6, pp. 591-606, https://doi.org/10.14256/JCE.3623.2022Jeta